Multiply Reflected Gaussian Beams in a Circular Cross Section

SANG-YUNG SHIN AND LEOPOLD B. FELSEN, FELLOW, IEEE

Abstract—A well-collimated beam reflected repeatedly within a circular cross section undergoes periodic focusing and defocusing. This behavior is of interest for tracking of beams around a type of acoustic surface wave disk delay line, and it also relates to beam monitoring after oblique injection into the endface of a multimode optical fiber. The problem is analyzed by considering first the field excited by an isotropic line source inside a dielectric cylinder, and then converting this to Gaussian beam excitation by assigning a complex value to the source coordinate location. Because the wavelength is small compared to the cylinder radius, ray-optical methods are employed to construct the solution, with inclusion of such novel ingredients as the lateral ray shift on a curved boundary. Results are obtained for the amplitude and phase of the ray and beam fields, and for such beam parameters as the location of the focus, the minimum beam width, and the rate of beam divergence between successive reflections.

I. Introduction and Summary

THE TRACKING of Gaussian beams undergoing successive total reflections at a concave boundary separating two dielectric media is of interest for several applications. In a type of acoustic surface wave delay line [1], a well-collimated acoustic beam is launched on the top surface of a circular piezoelectric disk so that it impinges obliquely on the rim. After traversing the rim, the beam passes across the underside of the disk, reemerges on the top side, and so on. This process can be modeled as multiple reflection at a circular boundary, with the effects of the rim accounted for by an equivalent boundary reflection coefficient. The utility of the device is dependent upon how well the multiply reflected beams remain collimated; the delayed signal cannot be extracted if the beam has too great a divergence. Although the piezoelectric disk is anisotropic, a first step requires the understanding of the beam behavior in an isotropic environment. The extension to anisotropy and (or) to noncircular rims has in fact already been accomplished [2] but is relegated to a future publication.

Another application is to optical communication where dielectric fiber waveguides with a homogeneous core are excited by a Gaussian beam injected obliquely across the fiber endface. This problem has been treated in the literature by guided-mode analysis [3]. However, for optical fiber waveguides with a large core diameter, the direct tracking of a beam reflected successively at the core boundary is relevant since the spot size of a focused incident beam is then small compared to the fiber cross section and requires the superposition of many guided modes. It may therefore be advantageous to track the incident beam directly into the fiber rather than to express the field at the outset in terms of a modal expansion. The conversion to guided modes may be performed at that location along the waveguide where the multiply reflected beams can no longer be individually resolved. The three-dimensional tracking problem may be better understood with *a priori* knowledge of the behavior of the cross-sectional fields. While the multiply reflected beam in a waveguide with constant refractive index continues to expand in the axial direction, the concave curvature of the boundary causes successive refocusing in the cross-sectional plane. Such refocusing of the three-dimensional beam field, and indeed its basic cross-sectional characteristics, are contained fully within the axially independent solution for a sheet beam that is launched in a circular domain. The results developed here have subsequently been employed for three-dimensional analysis [4].

Finally, the two-dimensional beam solution is of interest for application to curved layers encountered in integrated optics, when the beam field is injected, so as to cling to the outer boundary (whispering gallery type of propagation).

To effect the solution of the beam problem, we employ a recently formulated new technique whereby an incident two-dimensional Gaussian beam is generated from an incident line source (cylindrical wave) field by assigning complex values to the source coordinates [5]. Thus the Green's function problem, long of interest in radiation and diffraction theory, is also fundamental for the calculation of fields due to Gaussian beams. For the applications addressed here, attention is focused on high-frequency asymptotic solutions. These can be developed directly by ray-optical methods, without the need for departing initially from an exact formulation of the field problem. Apart from yielding the desired information directly, the ray-optical method is important because it can, within the present context, accommodate geometries, such as noncircular domains and(or) anisotropic material, for which exact solutions are not available.

While the complex-source-point technique converts the ray-optical field into a general beam field, it is adequate (for beams that remain well collimated) to consider only the paraxial region surrounding the beam axis since the field elsewhere is very small. Under these conditions, it suffices to restrict the source-excited ray-optical field to the vicinity of a central ray that subsequently becomes the

Manuscript received July 12, 1977; revised December 5, 1977. This work was supported by the National Science Foundation under Grant Eng 75-22625.

S. Y. Shin was with the Department of Electrical Engineering, Polytechnic Institute of New York, Farmingdale, NY 11735. He is now with the Korean Advanced Institute of Science, Seoul, Korea.

L. B. Felsen is with the Department of Electrical Engineering, Polytechnic Institute of New York, Farmingdale, NY 11735.

0018-9480/78/1100-0845$00.75 ©1978 IEEE

beam axis, i.e., it is adequate to treat a particular thin ray bundle rather than the entire family of rays. It is then found that the real parameters governing the phase and amplitude behavior of the field in the ray bundle also describe the field in the Gaussian beam when the analytic continuation to complex source point coordinates is performed. Thus, as in the parallel plane case [6], a rigorous link is provided between point-source-excited ray optics and paraxial beam optics, in terms of the conventional ray-optical parameters which have strong physical content. This aspect facilitates examination of the multiply reflected beam field solution with respect to periodic refocusing, beam spreading, and other physical attributes. Some numerical results provide further insight into these propagation phenomena.

Fundamental to the study of multiply reflected beams is the treatment of a single reflection. When, as in our case, the beam impinges at an angle larger than the critical angle for total reflection, the reflected beam emerges from a shifted position. This lateral shift for rays or beams, not previously explored for a curved boundary, has been developed and incorporated into our theory. While inclusion of the lateral shift may be inconsequential at a single reflection, the shifts accumulate for multiple reflections and are in fact essential when one wishes to convert the multiply reflected ray or beam fields into eigenmode fields in the circular cross section; omission of the lateral shift leads to an incorrect dispersion equation for the eigenmodes. These conclusions are similar to those noted previously for the planar geometry [6], and they have been confirmed by comparing the ray-optical fields employed here with the asymptotic solution of the rigorously formulated Green's function [7]. It should be emphasized that the remarks above apply to the general case where the refractive index contrast between the dielectric waveguide and the exterior may be substantial. For the optical fiber with small index difference between core and cladding, the effects of the lateral shifts are minimized.

The presentation is arranged as follows. Section II-A contains the two-dimensional ray-optical fields excited by an axial line source, their paraxial approximations in the vicinity of a preferred ray, and the effects of including or omitting the lateral shifts for totally reflected rays on a boundary with incidence-angle-dependent reflection coefficient. Some details pertaining to the ray-optical formulas are given in Appendix A, and the legitimacy of ignoring the ray shift for fields having undergone only a few reflections is demonstrated in Appendix B. The conversion of the line-source and point-source-excited fields to beam fields is performed in Section III. Included in the presentation are ray diagrams that provide a physical understanding of the behavior of the various field solutions and also numerical results for quantitative assessment of the evolution of the multiply reflected beam profile. The discussion of these results in Section IV provides further insight into the beam behavior.

II. Ray-Optical Fields

A. General Ray-Optical Fields

The incident field due to an electric line source in an unbounded dielectric is normalized so that G_{inc} is the infinite space Green's function

$$G_{\text{inc}}=\frac{i}{4}H_0^{(1)}(kD)\sim\frac{1}{4}\sqrt{\frac{2}{\pi kD}}\cdot\exp\,(ikD+i\pi/4),\qquad kD\gg 1 \tag{1}$$

where k is the wavenumber in the medium and D is the distance from the source. A time dependence $\exp(-i\omega t)$ is suppressed. Then the axial electric field G along a ray after a single reflection at the wall with radius "a" is given in [8]. As shown in Appendix A, the ray-optical field after s reflections can be constructed in a similar manner by ray tracing and monitoring the ray tube cross section. The result is

$$G\sim\frac{i}{4}\sqrt{\frac{2}{\pi k}}\,\left|\frac{L_{f0}}{L-L_{f0}}\right|^{1/2}\frac{1}{L_0^{1/2}}|\Gamma(\gamma_a)|^s e^{ik\psi}e^{-i(\pi/2)\sigma_f-i(\pi/4)} \tag{2}$$

where

$$\psi=2sL_a-L_0+L+s\theta(\gamma_a) \tag{2a}$$

and $\Gamma(\gamma_a)=|\Gamma(\gamma_a)|\exp\,[i\theta(\gamma_a)]$ is the boundary reflection coefficient. The lengths L_0, L_{f0}, L_a, and L, defined in Fig. 1, are measured from the perpendicular bisector of the central ray (shown dashed) in a ray tube: $L_a=a\sin\gamma_a$ is the half length of the central ray between reflections, L_0 locates the source point S, L_{f0} is the distance to a ray tube focus (point of tangency of the central ray with the caustic of the reflected ray family, which is not shown), and L is the distance to an observation point. The focal distance is given by

$$L_{f0}=L_aL_0(L_a-2sL_0)^{-1}\ \text{or}\ \frac{1}{L_{f0}}=\frac{1}{L_0}-\frac{2s}{L_a}. \tag{3}$$

Thus the focus moves toward the center of the reflected ray cord (i.e., $L_{f0}\to 0$) as the number s of reflections increases sufficiently. The orientation of the central ray is fixed by the angle γ_a. Depending on location along the multiply reflected ray, L and L_{f0} may be positive or negative; in regions 1, they are positive, while in regions 2, they are negative. Focusing need not occur after every reflection (σ_f counts the number of times that the central ray passes through a ray tube focus). In fact, a real focus $L=L_{f0}$ is possible only when L and L_{f0} have the same algebraic sign, and when $|L_{f0}|<L_a$; otherwise, there will be a virtual focus. The following rule concerning solutions of the equation $L=L_{f0}$ is found to apply:

$$\begin{aligned}
&s>(L_a/2L_0)+1/2, && \text{real focus in region 1}\\
&s<(L_a/2L_0)-1/2, && \text{real focus in region 2}\\
&\frac{L_a}{2L_0}-\frac{1}{2}<s<\frac{L_a}{2L_0}+\frac{1}{2}, && \text{no real focus.}
\end{aligned} \tag{4}$$

It may also be noted from (3) that $2sL_0=L_a$ implies that

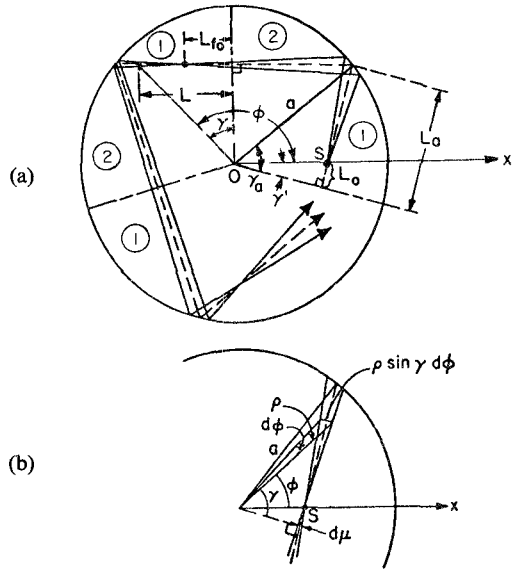

Fig. 1. Multiply reflected ray and ray tube (without lateral shift). (a) Multiply reflected ray. (b) Calculation of ray tube cross section (see Appendix A).

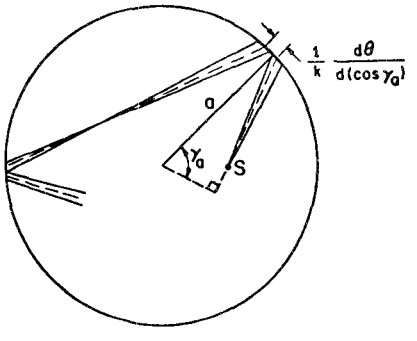

Fig. 2. Multiply reflected ray and ray tube (with lateral shift).

the reflected ray tube, after s reflections and before the next reflection, is made up of parallel rays.

After total reflection at the wall, the ray emerges with an amplitude modified by the reflection coefficient [7]

$$\Gamma(\gamma_a)\approx\frac{\sin\gamma_a-i(\cos^2\gamma_a-n^2)^{1/2}(1-i\delta)}{\sin\gamma_a+i(\cos^2\gamma_a-n^2)^{1/2}(1-i\delta)} \equiv|\Gamma(\gamma_a)|\exp[\,i\theta(\gamma_a)\,] \quad (5)$$

where the relative refractive index n is smaller than unity and

$$\delta=\exp\left\{-2ka\int_n^{\cos\gamma_a}\left[(\cos\gamma_a)^2/\tau^2-1\right]^{1/2}d\tau\right\}. \quad (5a)$$

The parameter δ arises from the leakage of the totally reflected incident ray field across the concave boundary; it is assumed that the leakage is small. Then to the first order in δ:

$$|\Gamma(\gamma_a)|=1-\frac{4\sin\gamma_a}{1-n^2}(\cos^2\gamma_a-n^2)^{1/2}\delta \quad (5b)$$

$$\theta(\gamma_a)=-2\tan^{-1}\left[(\cos^2\gamma_a-n^2)^{1/2}/\sin\gamma_a\right]. \quad (5c)$$

The total field at an observation point $\tilde{\rho}$, as computed by ray optics, is given by the sum of all fields along rays passing through $\tilde{\rho}$. This implies inclusion of all rays with such initial angles that they reach $\tilde{\rho}$ after an appropriate number of reflections. Formula (2) evidently fails when $L\to L_{f0}$ and must then be augmented by a caustic transition function [8]. For the present, we shall exclude such observation points from our considerations; this does not restrict, however, the subsequent complete description of the beam field (see (19)).

If the ray is to be tracked over many reflections, it is appropriate to employ the modified trajectories and fields obtained when the lateral ray shift L_ϕ on the boundary is included. In that event, the central ray is displaced (shown in Fig. 2) with the optical length ψ in (2a) modified to read

$$\psi=2sL_a-L_0+L+s\theta(\gamma_a)-\frac{s}{k}\frac{d\theta}{d(\cos\gamma_a)}\cos\gamma_a. \quad (6)$$

The ray shift is given by $L_\phi=-d\theta/dk_\phi$, where $k_\phi=k\cos\gamma_a$ is the wavenumber along the ϕ direction. This expression is inferred from the known shift for a plane boundary [6] by regarding the angular coordinate ϕ

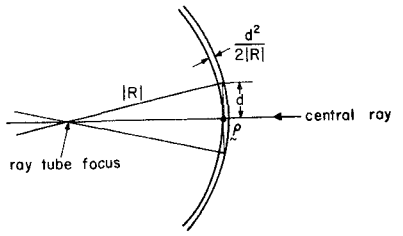

Fig. 3. Parameters for paraxial approximation.

at the point of impact of the ray as locally rectilinear. It can be shown [7] that L_ϕ determined by this procedure is in accord with the rigorously derived result. The corresponding phase accumulation at each reflection is then $k_\phi L_\phi$ as in (6). The term $|L_{f0}(L-L_{f0})^{-1}|$ in (2) becomes (see Appendix A)

$$\left|\frac{L_{f0}}{L-L_{f0}}\right| \to \left|\frac{L_{f0}}{L-L_{f0}-\frac{s}{k}\frac{LL_{f0}}{a^2}\frac{d^2\theta}{d(\cos\gamma_a)^2}}\right|. \quad (7)$$

The lengths L, L_0, and L_{f0} are now measured along the new trajectories.

It can be shown that, at a given observation point, the field computed from (2) and (5) with the nonshifted path in Fig. 1 agrees with the field computed from (6) and (7) with the laterally shifted path in Fig. 2 provided that the number of reflections is small and that $L \neq L_{f0}$. This is analogous to the result found previously for the plane stratified layer problem [6]; the derivation is sketched in Appendix B. Elsewhere [6], [7] we have performed a calculation whereby the multiply reflected ray fields are summed into guided modes and have shown that the laterally shifted paths must be utilized in order to obtain the correct asymptotic modal dispersion equation. However, for ray tracing with only a few reflections, the conventional nonshifted ray paths can be retained.

B. Paraxial Approximation

The ray-optical fields in (2) or their ray-shift-modified form in (6) and (7) are now expressed so that they describe observation points in the vicinity of the central ray in terms of quantities pertaining to that ray. This is accomplished by expanding the phase along a neighboring ray in terms of the parameters for the central ray (the ray amplitude is insensitive to this correction). Thus introducing a perpendicular distance d from a point $\tilde{\rho}$ on the central ray to an observation point $\tilde{\rho}=(\tilde{\rho},d)$, one finds that, without inclusion of the lateral shift (see Fig. 3),

$$\psi(\tilde{\rho},d)=2sL_a-L_0+L+\frac{d^2}{2R}+s\theta(\gamma_a), \qquad R=L-L_{f0} \quad (8)$$

provided that $d \ll |R|$. Subject to this modification, the formulas in (2) or in (6) and (7) describe the field in the paraxial region about the central ray defined by the angle γ_a. Note that R is the radius of curvature of the wavefront, positive for convex and negative for concave curvatures.

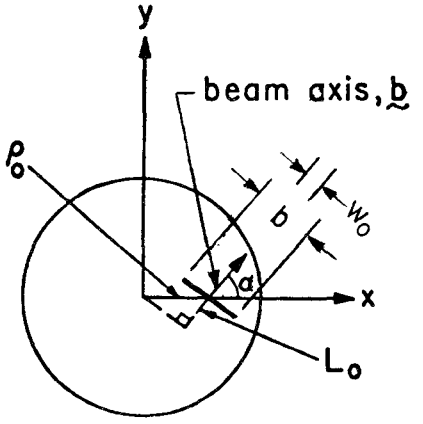

Fig. 4. Parameters for beam excitation.

When the lateral ray shift on the boundary is included, $\psi(\tilde{\rho},d)$ in (8) must be modified to read

$$\psi(\tilde{\rho},d)=2sL_a-L_0+L+\frac{d^2}{2\bar{R}}+s\theta(\gamma_a) - \frac{s}{k}\frac{d\theta}{d(\cos\gamma_a)}\cos\gamma_a \quad (8a)$$

where

$$\bar{R}=L-L_{f0}-\frac{s}{k}\frac{LL_{f0}}{a^2}\frac{d^2\theta}{d(\cos\gamma_a)^2}. \quad (8b)$$

III. Multiply Reflected Beam Fields

The preceding results for line-source-excited fields can be converted into excitation by a sheet beam by assigning a complex value to the source point. If the beam axis is inclined at an angle α with respect to the positive x axis and the beam waist is centered at x_0 thereon, one replaces [5] the real source point (x',y') by $(x_0+ib\cos\alpha, ib\sin\alpha)$, where b is a positive constant related to the beam width w_0 at the waist by $b=kw_0^2/2$ (see Fig. 4). Thus the polar source coordinates (ρ',ϕ') are transformed into

$$\rho'=(x'^2+y'^2)^{1/2}=\left[(\rho_0\cos\alpha+ib)^2+\rho_0^2\sin^2\alpha\right]^{1/2} \quad (9)$$

$$\phi'=\tan^{-1}\left(\frac{y'}{x'}\right)=\tan^{-1}\left(\frac{ib\sin\alpha}{\rho_0+ib\cos\alpha}\right) = \cos^{-1}\left(\frac{\rho_0\sin\alpha}{\rho'}\right)-\left(\frac{\pi}{2}-\alpha\right) \quad (10)$$

where $\rho_0=(x_0^2+y_0^2)^{1/2}=x_0$.

Since $\rho_0\cos\alpha=L_0$, one observes from the expression for ρ', and for ϕ' expressed in terms of ρ', that the above transformations from line source to beam fields can be accomplished by the replacement

$$L_0 \to L_0+ib. \quad (11)$$

The focal distance L_f becomes, accordingly,

$$L_f=\frac{L_a(L_0+ib)}{L_a-2s(L_0+ib)}=L_f^r+iL_f^i \quad (12)$$

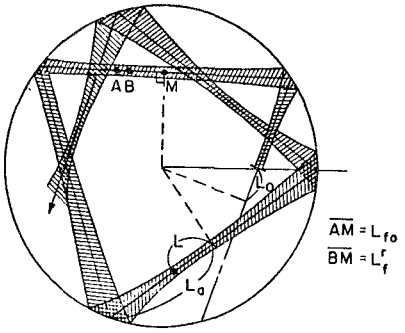

Fig. 5. Multiply reflected paraxial beam. A and B denote the locations of the ray tube foci and beam foci, respectively.

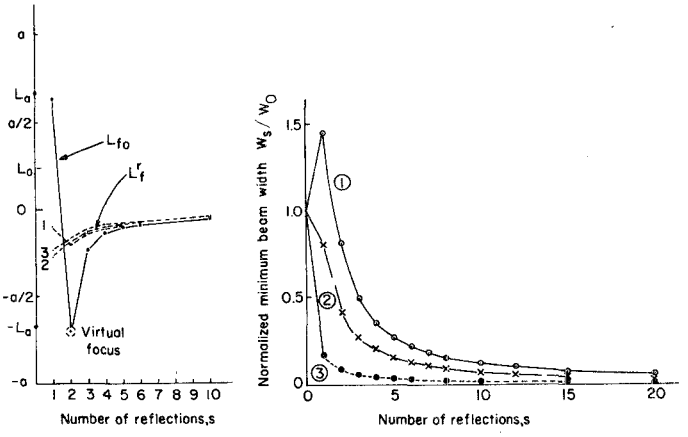

Fig. 6. Beam evolution after multiple reflection, for various relative beamwidths. In the curves shown, the incident beamwidth and incidence angle are held constant at $b=0.4$ and $\gamma=42^0$, respectively, while $L_0/a=0.22$. Curve 1: $a=2$; curve 2: $a=1$; curve 3: $a=0.2$. (a) Locations of minimum beamwidth L_f^r and ray tube focus L_{f0}; the ray tube focus between the first and second reflections lies exterior to the fiber core. (b) Relative minimum beamwidth w_s/w_0.

where

$$L_f^r = L_a \frac{L_0(L_a - 2sL_0) - 2sb^2}{(L_a - 2sL_0)^2 + 4s^2b^2} \tag{13}$$

$$L_f^i = b \frac{L_a^2}{(L_a - 2sL_0)^2 + 4s^2b^2}. \tag{14}$$

From (8), the paraxially approximated optical length becomes, omitting the lateral shift,

$$\psi_b = 2sL_a - (L_0 + ib) + L + \frac{d^2}{2(L - L_f^r - iL_f^i)}$$

$$= 2sL_a - (L_0 + ib) + L + \frac{d^2(L - L_f^r + iL_f^i)}{2(L - L_f^r)^2 + (L_f^i)^2}. \tag{15}$$

Defining the beamwidth w so that the exponential amplitude is expressed as $\exp(-d^2/w^2)$, one observes that the minimum beamwidth occurs at

$$L = L_f^r \tag{16}$$

rather than at the paraxial ray tube focus $L = L_{f0}$ (Fig. 5), and that

$$L_f^r - L_{f0} = 2sL_a^2b^2\left[(L_a - 2sL_0)^2 + 4s^2b^2\right]^{-1}(2sL_0 - L_a)^{-1}. \tag{17}$$

Note that after a sufficiently large number of reflections, the lengths L_f^r and L_{f0} become negative (i.e., the beam waist and the ray tube focus lie in region 2 of Fig. 1) and approach zero. However, there can be a marked difference between the two when the number of reflections is small and when $2sL_0 \approx L_a$ (see Fig. 6(a)).

The relative beamwidth w_s/w_0 at the minimum is given for $|L_f^r| < L_a$ by

$$w_s/w_0 = L_a\left[(2sL_0 - L_a)^2 + 4s^2b^2\right]^{-1/2}, \qquad w_0 = (2b/k)^{1/2} \tag{18}$$

with w_0 denoting the initial beamwidth at L_0 in Fig. 5. After many reflections, the minimum beamwidth tends to zero as shown in Fig. 6(b), and the field amplitude tends to zero since $L_f \to 0$. The latter circumstance implies a rapid divergence of the beam after many reflections. In (16), the location of the minimum beamwidth after s reflections has been based on the exponential behavior only, without inclusion of the algebraic terms in (19).

The total paraxial beam field is from (2), for $d \ll |L - L_f|$,

$$G_b \sim \frac{i}{4}\sqrt{\frac{2}{\pi k}}\left(\frac{L_f}{L - L_f}\right)^{1/2} \cdot \frac{1}{(L_0 + ib)^{1/2}} |\Gamma(\gamma_a)| e^{ik\psi_b - i\pi/4}, \qquad L_f = L_f^r + iL_f^i \tag{19}$$

with the square roots so defined that $G_b \to G$ in (2) when $b \to 0$. One observes that (19) remains valid at the beamwidth minimum so that, for the paraxial beam field, the restrictions imposed on the ray-optical formula (2) may be removed. Note, however, that since $L_f \to 0$ as $s \to \infty$, the resulting restriction $d \ll |L|$ prohibits observation points in the narrow focal region $L \to 0$, which then resembles that for the paraxial ray bundle (see (8)).

When the lateral shift on the boundary is included, the modified paraxial beam field is still given by (19) provided that (7), (8a), and (8b) are used with L_{f0} replaced by L_f. Calculations for application to optical fibers with the parameters in Fig. 6, based on the modified paraxial beam field, show no appreciable difference in the minimum beamwidth and the beam waist location along the shifted path. Shifted beam considerations can, however, be important after many reflections and for conversion of the multiply reflected beam field into azimuthally propagating eigenmodes [7].

The utility of beam tracking becomes questionable when the multiply reflected beams can no longer be individually resolved. It may then be preferable to employ the guided mode expansion. The limit of resolution in the circular cross section is somewhat less clearly defined than for the case of a slab waveguide [6]. Here, the degree of collimation of the beam may be taken as an appropriate

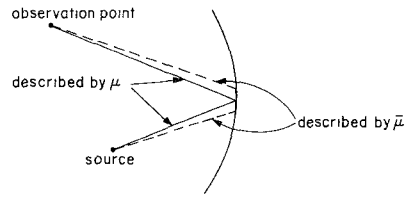

Fig. 7. Shifted and nonshifted ray paths for calculation of field after a single reflection.

measure of the utility of beam tracking. Since the angular divergence φ of a Gaussian beam is $\varphi = 2\tan^{-1}(2/kw_s)$, where w_s is the minimum spot size as given in (18), one may solve for the number of reflections s_c corresponding to a specified value of $C \equiv \tan(\varphi/2)$, recognizing that $kw_0 \gg 1$:

$$s_c \approx L_a \frac{L_0 + \sqrt{(L_0^2+b^2)\left(\frac{kw_0C}{2}\right) - b^2}}{2(L_0^2+b^2)}, \qquad b = \frac{kw_0^2}{2}. \tag{20}$$

When C is of the order of unity, the beam is strongly divergent, and the integer closest to s_c may then be taken to define a limit on the utility of the multiply reflected beam tracking procedure.

IV. Numerical Results

The behavior of the beam as it propagates between successive reflections at the circular wall is described by the normalized minimum beamwidth w_s/w_0 and the minimum beamwidth location as compared with the ray focus location. Numerical results are given in Fig. 6, for various relative beamwidths, by changing the radius of the circular cross section. From Fig. 6(a), it may be observed that for the smaller relative beamwidth (curve 1), the minimum beamwidth locations resemble those of the ray tube focus location. As the relative beamwidth is increased, the minimum beamwidth locations deviate markedly from the ray focus locations for the first few reflections, but their behavior becomes similar after many reflections. One observes from Fig. 6(b) that increasing the relative beamwidth (by decreasing the radius of the circular cross section) eventually decreases successive beamwidth minima w_s and hence increases the rate of beam divergence, as well as the rate at which L_f' approaches zero in Fig. 6(a). This behavior is attributed to the greater boundary curvature sampled by successively reflected beams under this condition. Though not plotted in the figure, one may also expect from (18) that as the waist of the injected beam moves closer to the boundary (i.e., for a larger L_0), the rate of beam divergence increases.

Appendix A
Derivation of the Ray-Optical Formulas

The formula in (2) can be constructed directly by ray-optical methods. First, one determines the ray paths and ray tubes shown in Fig. 1. In cylindrical (ρ, ϕ) coordinates, the ray path can be expressed as $\phi = \phi(\rho, \mu)$, where the ray parameter μ identifies the initial ray orientation γ_a via the relation $\mu = a\cos\gamma_a$. On a ray path, the functional dependence of ϕ on ρ is, for a ray incident in the counterclockwise direction (see Fig. 1(a)),

$$\phi = \gamma_> - \gamma_< + 2s\gamma_a + \phi' + 2n\pi \tag{21}$$

where (ρ', ϕ') locates the source point S and

$$\gamma_a = \cos^{-1}(\mu/a),\ \gamma_> = \cos^{-1}(\mu/\rho_>),\ \gamma_< = \cos^{-1}(\mu/\rho_<) \tag{21a}$$

with $\rho >$ and $\rho <$ denoting the greater or smaller values, respectively, of the radial observation point location ρ and source point location ρ'. The integer n indicates the number of ray circulations around the cylinder.

The ray tube cross section is calculated from Fig. 1(b) as

$$dA = \rho\sin\gamma\, d\phi = (\rho\sin\gamma)\, d\mu (d\phi/d\mu)_{\rho=\text{const.}} = \left|\frac{L - L_{f0}}{L_{fo}}\right| d\mu \tag{22}$$

where $\mu = a\cos\gamma_a = \rho\cos\gamma$ characterizes the central ray and $d\mu$ is constant along a ray tube. The ray tube cross section is conveniently tracked along ρ = constant contours, for which $d\phi/d\mu$ is then evaluated from (21); this leads to the last equality in (22). The procedure remains valid when ϕ in (21) is modified to account for the ray shift upon reflection by adding the term $-(s/k)(d\theta/d\mu)$ to the right-hand side. Equation (22) then becomes modified as in (7).

The ray-optical field is calculated from the well-known formula

$$u \sim \hat{u} e^{ik(\psi - \hat{\psi})} \sqrt{\frac{d\hat{A}}{dA}} \tag{23}$$

where the caret superscript identifies conditions at an initial reference point along a ray. The initial field can be referred to the source point (or focal point) by the relation

$$\hat{u} e^{-ik\hat{\psi}} \sim \frac{1}{4}\sqrt{\frac{2}{\pi k L_0}}\ \exp(i\pi/4) \tag{24}$$

which, upon inclusion also of the phase shifts at a caustic and the amplitude and phase change due to reflection, reduces (23) to (2). It has been verified [7] that this ray-optical result agrees with the asymptotic expansion of the rigorous solution.

APPENDIX B
REFLECTED FIELD EVALUATION ALONG CONVENTIONAL AND LATERALLY SHIFTED PATHS

In our previous analysis of propagation in plane stratified layers [6], we have shown that while the laterally shifted ray path must be employed when a ray undergoes a large number of reflections, the conventional nonshifted path is adequate to describe fields that have experienced one or a few reflections. We shall now demonstrate that the same conclusion is reached for the curved interface considered in this paper. Proceeding as before [6], we compare the total reflected field phase at a given observation point as computed from the phase function $Q(\mu)=[\psi(\mu)+s\theta(\mu)/k]$ for the nonshifted ray path with that from the phase function $Q(\bar{\mu})$ for the laterally shifted ray path (Fig. 7); the values μ and $\bar{\mu}$ for the two paths differ slightly by the amount $\Delta=\bar{\mu}-\mu$. When $\psi(\mu+\Delta)$ is expanded in a power series in Δ, one may show that

$$\Delta=-(d\theta/d\mu)(d^2\psi/d\mu^2+sd^2\theta/kd\mu^2)^{-1}. \tag{25}$$

Comparing $Q(\mu)$ and $Q(\bar{\mu})$, one finds them to be equivalent provided that

$$|(sd\theta/d\mu)^2[2(d^2Q/d\mu^2)]^{-1}|\ll 1. \tag{26}$$

Translated into geometrical terms (see Fig. 1), condition (26) becomes

$$\left|\frac{(sd\theta/d\mu)^2 LL_{f0}}{k(L-L_{f0})}\right|\ll 1 \tag{27}$$

provided that $L\gtrsim L_{f0}$ and $d\theta/d\mu$, $d^2\theta/d\mu^2$ are not excessively large.

REFERENCES

[1] I. M. Mason, "Acoustic-surface wave disk delay lines," *Proc. IEEE*, vol. 64, pp. 610–612, 1976.

[2] S. Y. Shin and L. B. Felsen, "Gaussian beam propagation on an acoustic surface wave disk delay line," in preparation.

[3] D. Marcuse, *Light Transmission Optics*. New York: Van Nostrand-Reinhold, 1972.

[4] S. Y. Shin and L. B. Felsen, "Beam evolution along a multimode optical fiber," presented at AGARD Symp. Optical Fibers, Integrated Optics, and their Military Applications, London, England, May 1977.

[5] L. B. Felsen, "Evanescent waves," *J. Opt. Soc. Am.* vol. 66, pp. 751–760, 1976.

[6] L. B. Felsen and S. Y. Shin, "Rays, beams, and modes pertaining to the excitation of dielectric waveguides," *IEEE Trans.*, vol. *MTT-23*, pp. 150–161, 1975.

[7] S. Y. Shin and L. B. Felsen, "Excitation of modes by a beam in a dielectric cylinder waveguide," in preparation.

[8] L. B. Felsen and N. Marcuvitz, *Radiation and Scattering of Waves*. Englewood Cliffs, NJ: Prentice-Hall, 1973, pp. 168–169, Sec. 5.8.